RSC Advances

ROYAL SOCIETY
OF CHEMISTRY

www.rsc.org/advances

Magnetic structure of $(C_5H_{12}N)CuBr_3$: Origin of the uniform Heisenberg chain behavior and the magnetic anisotropy of the Cu^{2+} (S = 1/2) ions

Changhoon Lee[1,2,3], Jisook Hong[2], Won-joon Son[4], Erjun Kan[5], Ji Hoon Shim[2,3,]*, and Myung-Hwan Whangbo[1,]*

[1]*Department of Chemistry, North Carolina State University, Raleigh, North Carolina 27695-8204, USA*

[2] *Department of Chemistry, Pohang University of Science and Technology, Pohang 790-784, Korea*

[3] *Division of Advanced Nuclear Engineering, Pohang University of Science and Technology, Pohang 790-784, Korea*

[4] *Samsung Advanced Institute of Technology, Suwon, Gyeonggi-do, South Korea, 443-803, Korea*

[5] *Department of Applied Physics and Key Laboratory of Soft Chemistry and Functional Materials (Ministry of Education), Nanjing University of Science and Technology, Nanjing, Jiangsu 210094, P. R. China.*

Abstract

The magnetic properties and electric polarization of the organic/inorganic hybrid system $(C_5H_{12}N)CuBr_3$ ($C_5H_{12}N$ = piperidinium) were examined on the basis of density functional theory calculations. The spin exchanges of $(C_5H_{12}N)CuBr_3$ evaluated by energy-mapping analysis show that its uniform Heisenberg antiferromagnetic chain behavior is not caused by the $CuBr_3$ chains made up of edge-sharing $CuBr_5$ square pyramids, but by the two-leg spin ladders resulting from interchain interactions. The magnetic anisotropy of the Cu^{2+} ions in $(C_5H_{12}N)CuBr_3$ originates largely from the Br^- ligands rather than the Cu^{2+} ions. The electric polarization of $(C_5H_{12}N)CuBr_3$ arises from the absence of inversion symmetry in the crystal structure, and is weakly affected by the magnetic structure.

1. Introduction

Recently a metal organic complex $(C_5H_{12}N)CuBr_3$ $(C_5H_{12}N$ = piperidinium) were synthesized, and its crystal and magnetic structures were investigated.[1] The structural building units of $(C_5H_{12}N)CuBr_3$, which crystallizes in a monoclinic space group C_2/c, are distorted $CuBr_5$ square pyramids conaining Cu^{2+} (d^9, S = 1/2) ions with three nonequivalent Br atoms (**Fig. 1a**). (Precisely speaking, the four basal Br atoms of each $CuBr_5$ are not coplanar but form a butterfly shape with *trans* $\angle$Br-Cu-Br = 151.50° and 177.95°.) The $CuBr_5$ pyramids share their basal edges to form Cu_2Br_8 dimers (**Fig. 1a**), which in turn share their non-basal edges to form $CuBr_3$ chains (**Fig. 1b**) running along the c-direction, and these chains are surrounded by the $C_5H_{12}N$ cations (**Fig. 2**). $(C_5H_{12}N)CuBr_3$ has no inversion symmetry in crystal structure, so it would be polar regardless of whether its Cu^{2+} spins undergo a magnetic ordering or not. However, it is of interest to examine how strongly the electric polarization of $(C_5H_{12}N)CuBr_3$ is infuenced by its magnetic structure.

The temperature-dependent magnetic susceptibility measured for powder samples of $(C_5H_{12}N)CuBr_3$ is well described by a Heisenberg uniform antiferromagnetic (AFM) chain model down to 1.8 K, and $(C_5H_{12}N)CuBr_3$ undergoes a three-dimensional (3D) magnetic ordering below T_N = 1.68 K.[1] The magnetic orbital of each $CuBr_5$ square pyramid is the x^2-y^2 orbital lying in the basal plane of the pyramid (**Fig. 3a**). Thus, within each $CuBr_3$ chain, there are two different nearest-neighbor spin exchanges. In the exchange path J_1, the two magnetic orbitals can interact strongly because they are coplanar (**Fig. 1b**). In the exchange path J_2, the two magnetic orbitals cannot interact strongly because they are not coplanar (**Fig. 1b**). Consequently, the spin exchanges J_1 and J_2 cannot be identical so that the $CuBr_3$ chains cannot be responsible for the uniform AFM chain behavior observed in experiments. A chosen spin-lattice such as the Heisenberg uniform AFM chain model should be consistent with its the electronic structure, which determines the magnetic energy spectrum.[2,3]

Experimentally, the spin-exchange parameters of a chosen spin-lattice are determined as the fitting parameters that simulate well the experimental magnetic data. However, the correctness of a chosen spin-lattice is not necessarily guaranteed even if it provides a good fitting as found for $(VO)_2P_2O_7$,[4,5] $Na_3Cu_2SbO_6$ and $Na_2Cu_2TeO_6$,[6-10] $Bi_4Cu_3V_2O_{14}$,[11-14] and $Cu_3(CO_3)_2(OH)_2$,[15,16] to name a few. To find what spin exchange paths of $(C_5H_{12}N)CuBr_3$ are responsible for its uniform antiferromagnetic AFM chain behavior, it is necessary to evaluate the intrachain as well as the interchain spin exchanges (**Fig. 1**).

Another interesting magnetic property of $(C_5H_{12}N)CuBr_3$ is its magnetic anisotropy. The magnetic susceptibilities measured for single-crystal samples of $(C_5H_{12}N)CuBr_3$ with probe magnetic field applied along the b-, c- and a*-directions [1] show that the susceptibility is substantially stronger along the a*-direction than along the b- and c-directions. As depicted in **Fig. 1c**, the basal planes of the $CuBr_5$ square pyramids are approximately parallel to the bc*-plane. Thus, the preferred spin orientation of the Cu^{2+} ions in $(C_5H_{12}N)CuBr_3$ is expected to be perpendicular to the basal plane (easy-axis anisotropy), i.e., along the (a − c/2)-direction, although this direction was not probed experimentally. Many magnetic solids containing Cu^{2+} ions show typically the easy-plane anisotropy as found for $CuCl_2 \cdot 2H_2O$,[17,18] $CuCl_2$,[19,20] $CuBr_2$[21], $LiCuVO_4$[22] and Bi_2CuO_4.[18,23,24] For nearly six decades, it had been erroneously believed that spin-1/2 ions embedded in solids cannot have magnetic anisotropy arising from spin-orbit coupling (SOC), so their magnetic anisotropy is caused either by anisotropic spin exchange or by their magnetic dipole-dipole interactions.[25] It is true that SOC cannot generate magnetic anisotropy for *isolated* spin-1/2 ions. However, it is recently reported that the spin-1/2 ions *embedded* in solids do possess the SOC-driven magnetic anisotropy because the d-states of such ions are split by the crystal field of their surrounding ligands.[18] The easy-axis anisotropy, which the Cu^{2+} ions in $(C_5H_{12}N)CuBr_3$ appear to exhibit, is found for Li_2CuO_2.[26,27] Since their magnetic anisotropy is expected to be caused by the SOC-induced

interactions between the crystal-field split d-states,[3,18] we may speculate that the split d-states of the Cu^{2+} ions in $(C_5H_{12}N)CuBr_3$ differ from those of the Cu^{2+} ions in compounds showing in-plane anisotropy. Furthermore, since the SOC constant is greater for Br than for Cu by a factor of ~ 2.9,[28] we may also speculate that the Br ligands have an important role in the spin orientation of Cu^{2+} ion.

    In the present work we explore the three questions raised above on the basis of density functional theory (DFT) calculations. We evaluate the intrachain and interchain spin exchanges ($J_1 - J_6$) of $(C_5H_{12}N)CuBr_3$ by performing energy-mapping analysis to find that two-leg-spin ladders with strong AFM rung act effectively as uniform AFM chains. Our DFT calculations show that the easy-axis anisotropy of Cu^{2+} ions of $(C_5H_{12}N)CuBr_3$ is largely induced by the SOC of Br^- ligands rather than that of Cu^{2+}. Finally we show that the electric polarization of $(C_5H_{12}N)CuBr_3$ is not much affected by the change in its magnetic structure.

2. Computational details

    In our DFT calculations, we employed the frozen-core projector augmented wave method [29,30] encoded in the Vienna ab initio simulation package (VASP),[31] and the generalized-gradient approximation of Perdew, Burke and Ernzerhof [32] for the exchange-correlation functional with the plane-wave-cut-off energy of 450 eV and a set of 32 k-point for the irreducible Brillouin zone. To examine the effect of the electron correlation in the Cu 3d states, the DFT plus on-site repulsion method (DFT+U)[33] was used with the effective U_{eff} = U – J values of 2, 4, 6 and 8 eV. The preferred orientation of the Cu^{2+} spins in $(C_5H_{12}N)CuBr_3$ was determined by performing DFT+U calculations including the SOC.[34]

3. Spin exchange and spin lattice

Spin exchanges in magnetic solids of spin-1/2 Cu^{2+} ions are strongly governed by the arrangement of the square planes containing their magnetic orbitals.[2,3] J_1 and J_2 are of the Cu-Br-Cu exchange type, while $J_3 - J_6$ are of the Cu-Br···Br-Cu exchange type. J_1, J_2, and J_3 are intrachain exchanges, and the J_4, J_5, and J_6 are interchain exchanges. The geometrical arrangements of the exchange paths $J_1 - J_6$ is presented in **Fig. 5**. The geometrical parameters associated with the paths $J_1 - J_6$ are summarized in **Table 1**. In terms of the projected density of states (PDOS) plots the electronic structure calculated for the ferromagnetic (FM) state of $(C_5H_{12}N)CuBr_3$ is presented in **Fig. 6**. The PDOS plots of the Cu 3d and Br 4p orbitals, shown only for the down-spin (minority-spin) states for simplicity, are obtained by using the local Cartesian coordinated defined in **Fig. 6a**. The contribution to the unoccupied states come primarily from the x^2-y^2 orbital of Cu, the $4p_x$ orbitals of Br(1), $4p_y$ orbitals of Br(3), as well as the $4p_x/4p_y$ orbitals of Br(2). Each Br(2) has both $4p_x$ and $4p_y$ orbital contributions, because they make σ^* bonding combinations to the x^2-y^2 orbitals to the two different Cu atoms (**Fig. 6a**). This is consistent with the nature of the magnetic orbital expected for the Cu^{2+} (S = 1/2, d^9) ion of each $CuBr_5$ square pyramid (**Fig. 3a**).

To extract the values of $J_1 - J_6$ by energy-mapping analysis, we first calculate the six relative energies using the seven ordered spin states (FM, AF1 −AF6) of $(C_5H_{12}N)CuBr_3$, depicted in **Fig. S1**, on the basis of DFT+U calculations as summarized in the parentheses of **Fig. S1**. In terms of the spin Hamiltonian

$$\hat{H} = -\sum_{i<j} J_{ij}\hat{S}_i \cdot \hat{S}_j, \tag{1}$$

where $J_{ij} = J_1 - J_6$, the total spin exchange energies E_{spin} of these states per eight formula units (8FUs) are expressed as

$$E_{spin} = (n_1J_1 + n_2J_2 + n_3J_3 + n_4J_4 + n_5J_5 + n_6J_6)N^2/4 \tag{2}$$

by using the energy expressions obtained for spin dimers with N unpaired spins per spin site (in the present case, N = 1).[3,35] The values of $n_1 - n_7$ for the seven ordered spin states, FM and AF1 – AF6, are summarized in **Table S1**. Thus, by mapping the relative energies of the spin ordered states obtained from the DFT+U calculations onto the corresponding relative energies from the total spin exchange energies, we obtain the values of $J_1 - J_6$ summarized in **Table 2**.

Among the intrachain spin exchanges, J_1 is strongly AFM, J_2 is ferromagnetic (FM), and J_3 is negligible. Given that $\angle$Cu-Br-Cu = 95° and 90° for the J_1 and J_2 paths, respectively, it is not surprising that J_1 is AFM while J_2 is FM.[36] Clearly, then, the $CuBr_3$ chains do not form uniform AFM chains as anticipated. Among the interchain exchanges, J_4 and J_6 are weak, but J_5 is strongly AFM although the Cu...Cu distance is very long compared to the intrachain case. Note that uniform AFM chains should be formed along the b-direction with the J_5 exchange. In the Cu-Br...Br-Cu exchange J_5, the two magnetic orbitals are arranged as depicted in **Fig. 3b**. Thus, the overlap between the two magnetic orbitals across the Br...Br contact via the Br 4p magnetic orbital tails is strong, thereby leading to a strong AFM exchange. Note that two adjacent uniform chains made up of the interchain exchanges J_5 are linked by the intrachain exchanges J_1 to form two-leg spin ladders. Such ladders are linked by the FM intrachain exchanges J_2 to form 2D layers of the two-leg spin ladders parallel to the bc-plane, and these 2D layers are stacked along the a-direction (**Fig. 5**) with very weak interlayer exchange J_6 between them. J_6 is weakly FM for $U^{eff} < 5$ eV, but is weakly AFM for $U^{eff} > 5$ eV. In any event, the existence of a nonzero J_6 allows $(C_5H_{12}N)CuBr_3$ to undergo a 3D AFM ordering at low temperature as observed experimentally.[1]

For our discussion of the two-leg spin ladders, it is convenient to employ the new notations $J_\parallel = J_5$ for the leg and $J_\perp = J_1$ for the rung. **Table 2** shows that the $J_\perp/J_\parallel$ ratio changes from 4.7 to 0.95 as U^{eff} varies from 2 to 8 eV. When the rung exchange $J_\perp$ is considerably

greater than the leg exchange $J_\parallel$, the two-leg spin ladder would behave like a uniform AFM

chain, because the low-energy excitation spectrum would be dominated by the excitations

associated with the weaker exchange (i.e., $J_\parallel$), not with the stronger exchange (i.e., $J_\perp$).

To verify this point, we simulate the magnetic susceptibility using the Monte Carlo

method.[37,38] In this simulation we employed the values of the spin exchanges obtained from

the DFT+U calculations with U^{eff} = 6 eV. As shown in **Fig. 4**, the calculated magnetic

susceptibility is in good agreement with the experimental one. It is interesting to note that the

uniform AFM chain is formed along the interchain direction instead of the intrachain

direction.

4. Preferred spin orientation

To determine the preferred orientation of the Cu^{2+} spins in $(C_5H_{12}N)CuBr_3$, we carry

out DFT+U calculations including the SOC for sevel different spin orientations defined with

respect to the local Cartesian coordinate defined in **Fig. 1a,6a**. There are eight identical Cu^{2+}

ions per unit cell in $(C_5H_{12}N)CuBr_3$ but we simplify our calculations by replacing all but one

Cu^{2+} ions with nonmagnetic Mg^{2+} ions. Results of our DFT+U+SOC calculations for this

model are summarized in **Table 3**, which shows that the spin orientation along the local z-

direction is lower in energy, though slightly, than that any other direction. That is, the Cu^{2+}

(d^9) ions in $(C_5H_{12}N)CuBr_3$ have easy-axis anisotropy, as aready anticipated.

We now examine how the above result can be explained from the viewpoint of the

crystal-field split d-states of the $CuBr_5$ square pyramid. By employing the coordinate (x, y, z)

for the orbital momentum and the coordinate (x′, y′, z′) for the spin momentum, the SOC

term $\lambda\hat{S}\cdot\hat{L}$ is written as[3,39-41]

$$\hat{H}_{SO} = \lambda\hat{S}\cdot\hat{L} \approx \hat{H}_{SO}^0 = \lambda\hat{S}_{z'}\left(\hat{L}_z\cos\theta + \frac{1}{2}\hat{L}_+e^{-i\phi}\sin\theta + \frac{1}{2}\hat{L}_-e^{+i\phi}\sin\theta\right) \qquad (3)$$

where we omitted the terms that allow interactions between different spin states. The preferred spin orientation is given by the orientation of the z′-axis. If the z′-axis is along the z-axis (i.e., $\theta = 0°$), the magnetic ion has easy-axis anisotropy. If the z′-axis lies in the xy-plane (i.e., $\theta = 90°$), the magnetic ion has easy-plane anisotropy.

When an occupied up-spin (down-spin) d-state $\psi_o\uparrow$ ($\psi_o\downarrow$) of energy e_o interacts with an unoccupied up-spin (down-spin) d-state $\psi_u\uparrow$ ($\psi_u\downarrow$) of energy e_u via the matrix element $\langle\psi_o|\hat{H}^0_{SO}|\psi_u\rangle$, the associated energy lowering ΔE_{SOC} is given by

$$\Delta E_{SOC} = -\frac{\left|\langle\psi_o|\hat{H}^0_{SO}|\psi_u\rangle\right|^2}{|e_o - e_u|}. \tag{4}$$

Provided that the matrix elements $\langle\psi_o|\hat{H}^0_{SO}|\psi_u\rangle$ are comparable in magnitude, the most important interaction is the one involving the highest occupied (HO) and the lowest unoccupied (LU) states. To predict the preferred spin orientation using Eqs. (3) and (4), it is necessary to know at what spin orientation the term $\langle\psi_o|\hat{H}^0_{SO}|\psi_u\rangle$ is nonzero and can be maximized. The preference for the ∥z direction (easy-axis anisotropy) requires a nonzero $\langle\psi_o|\hat{L}_z|\psi_u\rangle$, while that for the ∥xy plane (easy-plane anisotropy) requires a nonzero $\langle\psi_o|\hat{L}_+|\psi_u\rangle$ or a nonzero $\langle\psi_o|\hat{L}_-|\psi_u\rangle$. In terms of the spherical harmonics Y_2^m (m = 0, ±1, ±2), the angular behaviors of the d-orbitals are given by $3z^2-r^2 \propto Y_2^0$, $xz \propto (Y_2^{-1} - Y_2^1)$, $yz \propto (Y_2^{-1} + Y_2^1)$, $xy \propto (Y_2^{-2} - Y_2^2)$, and $x^2-y^2 \propto (Y_2^{-2} + Y_2^2)$. Namely, the difference in the magnetic quantum numbers m (i.e., |Δm|) is 0 between xz and yz and between xy and x^2-y^2, |Δm| = 1 between $3z^2-r^2$ and {xz, yz} and between {xz, yz} and {xy, x^2-y^2}, and |Δm| = 2 between $3z^2-r^2$ and {xy, x^2-y^2}. Then, according to the relationship

$$\left\langle Y_2^n \left| \hat{L}_z \right| Y_2^m \right\rangle = \delta_{nm}$$

$$\left\langle Y_2^n \left| \hat{L}_+ \right| Y_2^m \right\rangle = \delta_{n(m+1)} \qquad (5)$$

$$\left\langle Y_2^n \left| \hat{L}_- \right| Y_2^m \right\rangle = \delta_{n(m-1)}$$

the interaction between two d-states under the SOC induces easy-axis anisotropy if $|\Delta m| = 0$, but easy-plane anisotropy if $|\Delta m| = 1$.

Therefore, the easy-axis anisotropy found for the Cu^{2+} ions of $(C_5H_{12}N)CuBr_3$ is explained if the SOC-induced interaction of the empty $x^2-y^2\downarrow$ states with the filled $xy\downarrow$ states is stronger than that with the filled $xz/yz\downarrow$ states. The PDOS plots of $(C_5H_{12}N)CuBr_3$ in **Fig. 6b** show that the empty $x^2-y^2\downarrow$ orbitals are well separated from the filled $xz/yz\downarrow$ orbitals, and equally well separated from the filled $xy\downarrow$ orbitals. Using Eq. 4 and the PDOS plots of **Fig. 6b**, however, it is difficult to conclude that the preferred spin orientation is the local z-direction (i.e., easy-axis anisotropy). The latter implies that the SOC of Cu is not responsible for the easy-axis anisotropy. Since the SOC constant of Br is about three times greater than that of Cu, one might wonder if the SOC of Br plays a role in determining the prefered spin orientation of $(C_5H_{12}N)CuBr_3$. Thus we examine the Br 4p orbitals combined into the $xy\downarrow$ and $x^2-y^2\downarrow$ states (**Fig. 6c**). The Br 4p orbitals make π^* antibonding to the Cu xy orbital in the $xy\downarrow$ state (**Fig. 3c**), but make σ^* antibonding to the Cu x^2-y^2 orbitals in the $x^2-y^2\downarrow$ states (**Fig. 3a**). Thus, at any Br site of the $CuBr_5$ basal plane, the Br 4p orbital of the $xy\downarrow$ is orthogonal to that of the $x^2-y^2\downarrow$ state. At a given Br atom, these Br 4p orbitals can be taken to be $4p_x$ and $4p_y$ orbitals without loss of generality. As can be seen from **Fig. 6c**, the energy gap between the occupied and unoccupied Br 4p orbitals is much smaller than that between the occupied and unoccupied Cu d-orbitals. Thus, according to Eq. 4, the SOC effect of Br is more important than that of Cu. This conclusion is further reinforced by the facts that the

SOC constant is much greater for Br than for Cu, and that there are more Br than Cu aoms in

$(C_5H_{12}N)CuBr_3$.

The only nonzero matrix element for the SOC between the $4p_x$ and $4p_y$ orbitals

occurs for $\hat{L}_z$, namely, $\langle y|\hat{L}_z|x\rangle = i$.[40] Because this term comes with the factor $\cos\theta$ (Eq.

3), it is maximized when $\theta = 0°$. Therefore, the Br ligands associated with the SOC between

the $x^2-y^2\downarrow$ and $xy\downarrow$ states predict easy-axis anisotropy for $(C_5H_{12}N)CuBr_3$. Obviously, from

the SOC of the $x^2-y^2\downarrow$ states with the $xz\downarrow$ or $yz\downarrow$, one predicts in-plane anisotropy by

considering the SOC of the associated Br 4p orbitals. This explains why the magnetic

anisotropy is weak in $(C_5H_{12}N)CuBr_3$.

5. Polariztion

Since $(C_5H_{12}N)CuBr_3$ has the crystal structure with no inversion symmetry, it should

have a nonzero electric polarization. We calculate the electric polarization of $(C_5H_{12}N)CuBr_3$

for the magnetic ground state (i.e., the AF4 state) as well as hypothetical FM state by using

the Berry phase method [41,42] encoded in the VASP. For the electric polarization of

$(C_5H_{12}N)CuBr_3$, our DFT+U+SOC calculations give 0.17 and 0.19 $\mu C/m^2$ for FM and AFM

states, respectively. Thus, the electric polarization of $(C_5H_{12}N)CuBr_3$ is weakly affected by its

magnetic structure.

6. Concluding remarks

Our study shows that the uniform Heisenberg antiferromagnetic chain behavior of

$(C_5H_{12}N)CuBr_3$ is not caused by the $CuBr_3$ chains, but by the two-leg spin ladders resulting

from interchain interactions. The Cu^{2+} ions in $(C_5H_{12}N)CuBr_3$ have easy-axis anisotropy,

which arises largely from the Br⁻ ligands rather than the Cu^{2+} ions. $(C_5H_{12}N)CuBr_3$ has a

nonzero electric polarization, which is weakly affected by its magnetic structure.

Supporting information

       Table S1 as well as **Figure S1** are available free of charge via the Internet at http://

Acknowledgments

References

(1) B. Pan, Y. Wang, L. Zhang, S. Li, *Inorg. Chem.*, 2014, **53**, 3606.

(2) M. –H. Whangbo, H. –J. Koo, D. Dai, *J. Solid State Chem*. 2003, **176**, 417.

(3) H. J. Xiang, C. Lee, H. –J. Koo, X. G. Gong, M. –H. Whangbo, *Dalton Trans*. 2013, **42**, 823.

(4) A. W. Garret, S. E. Nagler, D. A. Tennant, B. C. Sales, T. Barnes, *Phys. Rev. Lett*. 1997, **79**, 745.

(5) H. –J. Koo, M. –H. Whangbo, P. D. VerNooy, C. C. Torardi, W. J. Marshall, *Inorg. Chem.* 2002, **41**, 4664.

(6) J. Xu, A. Assoud, N. Soheilnia, S. Derakhshan, H. L. Cuthbert, J. E. Greedan, M. –H. Whangbo, H. Kleinke, *Inorg. Chem*. 2005, **44**, 5042.

(7) Y. Miura, R. Hirai, Y. Kobayashi, M. Sato, *J. Phys. Soc. Jpn*. 2006, **75**, 84707.

(8) S. Derakhshan, H. L. Cuthbert, J. E. Greedan, B. Rahman, T. Saha-Dasgupta, *Phys. Rev. B* 2007, **76**, 104403.

(9) H. –J. Koo, M. –H. Whangbo, *Inorg. Chem*. 2008, **47**, 128.

(10) Y. Miura, Y. Yasui, T. Oyoshi, M. Sato, K. Kakurai, *J. Phys. Soc. Jpn*. 2008, **77**, 104789.

(11) H. Sakurai, K. Yoshimura, K. Kosuge, N. Tsujii, H. Abe, H. Kitazawa, G. Kido, H. Michor, G. Hilscher, *J. Phys. Soc. Jpn*. 2002, **71**, 1161.

(12) S. Okubo, T. Hirano, Y. Inagaki, H. Ohta, H. Sakurai, H. Yoshimura, K. Kosuge, *Physica B* 2004, **346**, 65.

(13) K. Okamoto, T. Tonegawa, M. Kaburagi, *J. Phys.: Condens. Matter* 2003, **15**, 5979.

(14) H. –J. Koo, M. –H. Whangbo, *Inorg. Chem*. 2008, **47**, 4779.

(15) K. C. Rule, A. U. B. Wolter, S. S€ullow, D. A. Tennant, A. Brouhl, S. Kohler, B. Wolf, M. Lang, J. Schreuer, *Phys. Rev. Lett*. 2008, **100**, 117202.

(16) J. Kang, C. Lee, R. K. Kremer, M. –H. Whangbo, *J. Phys.: Condens. Matter* 2009, **21**, 392201.

(17) N. J. Poulis, G. E. G. Haderman, *Physica* 1952, **18**, 201.

(18) J. Liu, H. –J. Koo, H. J. Xiang, R. K. Kremer, M. –H. Whangbo, *J. Chem. Phys*. 2014, **141**, 124113.

(19) M. G. Banks, R. K. Kremer, C. Hoch, A. Simon, B. Ouladdiaf, J. –M. Broto, H. Rakoto, C. Lee, M. –H. Whangbo, *Phys. Rev. B* 2009**, 80,** 024404.

(20) L. Zhao, T. –L. Hung, C. –C. Li, Y. –Y. Chen, M. –K. Wu, R. K. Kremer, M. G. Banks, A. Simon, M. –H. Whangbo, C. Lee, J. S. Kim, I. G. Kim, K. H. Kim, *Adv. Mater*. 2012, **24**, 2469.

(21) (a) D. Dai, H. –J. Koo, M. –H. Whangbo, *Inorg. Chem.* 2004, **43**, 4026. (b) H. –J. Koo, C. Lee, M. –H. Whangbo, G. J. McIntyre, R. K. Kremer, *Inorg. Chem.* 2011, **50**, 3582.

(22) B. J. Gibson, R. K. Kremer, A. V. Prokofiev, W. Assmus, G. J. McIntyre, *Physica B* 2004, **350**, e253.

(23) K. Yamada, K. –I. Takada, S. Hosoya, Y. Watanabe, Y. Endoh, N. Tomonaga, T. Suzuki, T. Ishigaki, T. Kamiyama, H. Asano, F. Izumi, *J. Phys. Soc. Jpn.* 1991, **60**, 2406.

(24) M. Herak, M. Miljak, G. Dhalenne, A. Revcolevschi, *J. Phys.: Condens. Matter.* 2010, **22**, 026006.

(25) T. Moriya, K. Yoshida, *Prog. Theoret. Phys.* 1953, **9**, 663.

(26) F. Sapina, J. Rodriguez-Carvajal, M. J. Sanchis, R. Ibanez, A. Beltran, D. Beltran, *Solid State Commun.* 1990, **74**, 779.

(27) E. M. L. Chung, G. J. McIntyre, D. McK. Paul, G. Balakrishnan, M. R. Lees, *Phys. Rev. B* 2003, **68**, 144410.

(28) M. Montalti, A. Credi, L. Prodi, M. T. Gandolphi, *Handbook of Photochemistry, Third Edition*, CRC Press, Taylor Francis Group, Boca Raton, Florida, 2006, Table 13a.

(29) P. E. Blöchl, *Phys. Rev. B* 1994, **50**, 17953.

(30) G. Kresse, D. Joubert, *Phys. Rev. B* 1999, **59**, 1758.

(31) G. Kresse, J. Furthmüller, *Phys. Rev. B* 1996, **54**, 11169.

(32) J. P. Perdew, K. Burke, M. Ernzerhof, *Phys. Rev. Lett.* 1996, **77**, 3865.

(33) S. L. Dudarev, G. A. Botton, S. Y. Savrasov, C. J. Humphreys, A. P. Sutton, *Phys. Rev. B* 1998, **57**, 1505.

(34) J. Kuneš, P. Novák, R. Schmid, P. Blaha and K. Schwarz, *Phys. Rev. B* 2001, **64**, 153102.

(35) D. Dai, M. –H. Whangbo, *J. Chem. Phys.* 2001, **114**, 2887.

(36) J. B. Goodenough, *Magnetism and the Chemical Bond*, Interscience, 1963.

(37) P. S. Wang, W. Ren, L. Bellaiche, H. J. Xiang, *Phys. Rev. Lett.* **2015**, *114*, 147204

(38) We carried out parallel tempering Monte Carlo (PTMC) simulations. See: K. Hukushima,

K. Nemoto, *J. Phys. Soc. Jpn*. 1996, **65**, 1604.

(39) X. Wang, R. Wu, D. –S. Wang, A. J. Freeman, *Phys. Rev. B* 1996, **54**, 61.

(40) D. Dai, H. J. Xiang, M. –H. Whangbo, *J. Comput. Chem*. 2008, **29**, 2187.

(41) M.-H. Whangbo, E. E. Gordon, H. J. Xiang, H.-J. Koo and C. Lee, *Acc. Chem. Res.* **48**,

3080 (2015).

(42) R. D. King-Smith, D. Vanderbilt, *Phys. Rev. B* 1993, **47**, 1651.

(43) R. Resta, *Rev. Mod. Phys*. 1994, **66**, 899.

Table 1. Geometrical parameters associated with the exchange paths $J_1 - J_6$ in $(C_5H_{12}N)CuBr_3$.

The lengths and angles are in units of Å and degrees, respectively.

	Cu-Cu	Cu-Br	Br...Br	∠Cu-Br-Cu	∠Cu-Br-Br
J_1	3.622	2.462 (×2) 2.449 (×2)		95.0	
J_2	3.712	2.423 (×2) 2.802 (×2)		90.2	
J_3	6.673	2.423 2.462	4.009		100.5 93.9
J_4	7.348	2.412 (×2) 2.463 (×2)	4.220 (×2) 3.929		104.0 161.9 113.8
J_5	8.835	2.449(×2)	4.220		154.6 161.9
J_6	9.357	2.412 2.423	6.560		119.5 117.6

Table 2. Values of the spin exchanges $J_1 - J_6$ (in k_BK) of $(C_5H_{12}N)CuBr_3$ obtained from the DFT+U Calculations with effective U^{eff} (in eV).

	$U^{eff} = 2$	$U^{eff} = 4$	$U^{eff} = 6$	$U^{eff} = 8$
J_1	-197.6	-105.9	-52.3	-21.4
J_2	12.1	14.4	15.1	14.6
J_3	-5.7	-4.1	-3.1	-2.5
J_4	-9.5	-4.5	-4.5	-3.5
J_5	-41.8	-33.7	-27.1	-22.6
J_6	0.05	0.02	-0.04	-0.25

Table 3. Relative energies (in k_BK per Cu) of various orientations of the Cu^{2+} spin in $(C_5H_{12}N)CuBr_3$ obtained from the DFT+U+SOC calculations with effective U^{eff} (in eV). The spin orientation is defined using the local Cartesian coordinate (Fig. 1a, 5a).

Orientation	$U^{eff} = 2$	$U^{eff} = 4$	$U^{eff} = 6$
x	0.0	0.0	0.0
y	-0.3	-0.4	-0.5
z	-1.4	-1.7	-2.1
x+z	-0.5	-0.7	-0.9
y+z	-0.6	-0.8	-1.0

Figure captions

Figure 1. Structural features of $(C_5H_{12}N)CuBr_3$, where the Cu and Br atoms are represented by blue and grey spheres, respectively (a) Cu_2Br_8 dimer unit made up of two $CuBr_5$ square pyramids by sharing their basal edges, where the numbers 1, 2 and 3 refer to Br(1), Br(2) and Br(3), respectively. (b) $CuBr_3$ chain obtained from Cu_2Br_8 dimers by sharing their non-basal edges. (c) Arrangements of Cu_2Br_8 dimer units in the bc*-plane, where the apical Br atoms are removed for clarity. (d) Arrangement of two $CuBr_3$ chains. The numbers 1 – 6 in (b) – (d) refer to the spin exchange paths $J_1 – J_6$, respectively.

Figure 2. Two views of how the $CuBr_3$ chains are packed with $C_5H_{12}N^+$ cations in $(C_5H_{12}N)CuBr_3$: Projection views (a) along the c-direction and (b) along the b-direction. The pink polyhedra, black, gray, and blue circles are represent the $CuBr_5$ units, H, C, and C atoms, respectively.

Figure 3. (a) The $x^2–y^2$ state of a Cu^{2+} ion at a square planar, a square pyramidal or an octahedral site. (b) Arrangement of two $x^2–y^2$ magnetic orbitals leading to a strong antiferromagnetic interaction. (c) The xy state of a Cu^{2+} ion at a square planar, a square pyramidal or an octahedral site.

Figure 4. Temperature-dependent magnetic susceptibility of $(C_5H_{12}N)CuBr_3$, χ, calculated by using the Monte Carlo method on the basis of the classical spin Hamiltonian defined in terms of the spin exchange constants obtained from DFT+U calculations ($U^{eff} = 6.0$ eV). The inset shows the experimental magnetic susceptibility taken from ref. 1.

Figure 5. Arrangements of the spin exchange paths in $(C_5H_{12}N)CuBr_3$: (a) A layer made up of the exchange paths $J_1 - J_5$. (b) Arrangement of the exchanges $J_1 - J_6$ forming a 3D lattice.

Figure 6. PDOS plots obtained for the down-spin d-states in the FM state of $(C_5H_{12}N)CuBr_3$ from the DFT+U calculations with $U^{eff} = 4V$: (a) The local Cartesian coordinate used to obtain the PDOS plots. (b) The PDOS plots obtained for the Cu 3d orbitals. (c) The PDOS plots obtained for the Br 4p orbitals.
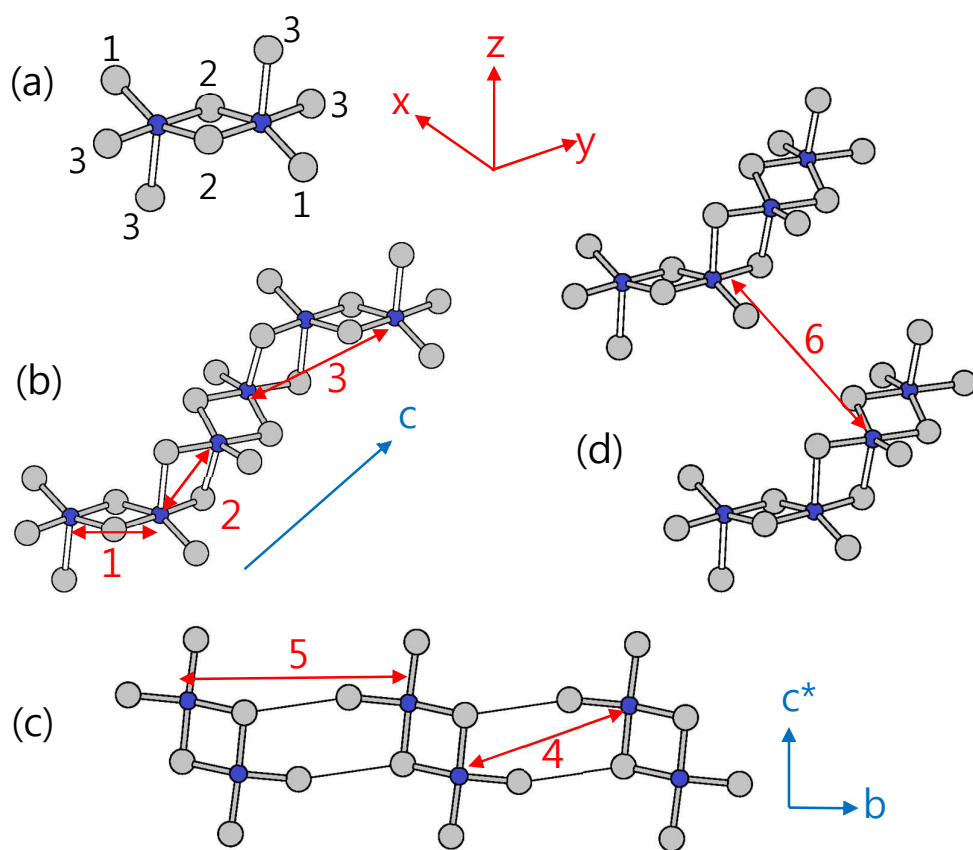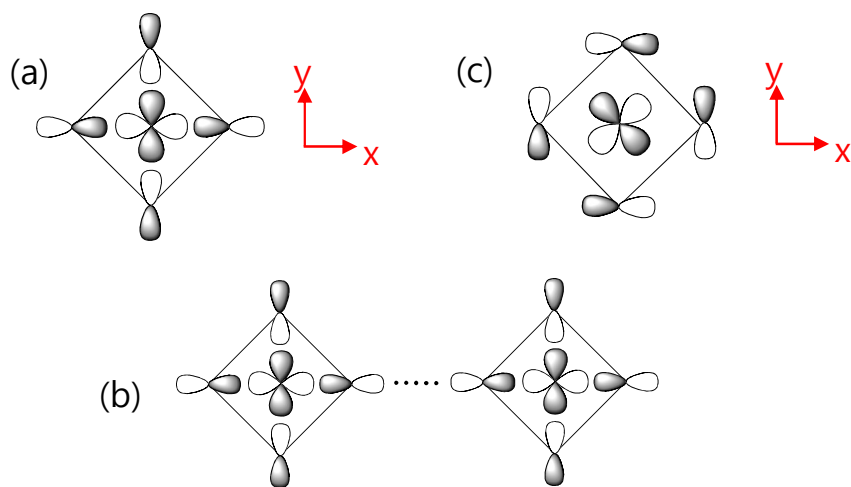
Figure 1.

(a)

(b)
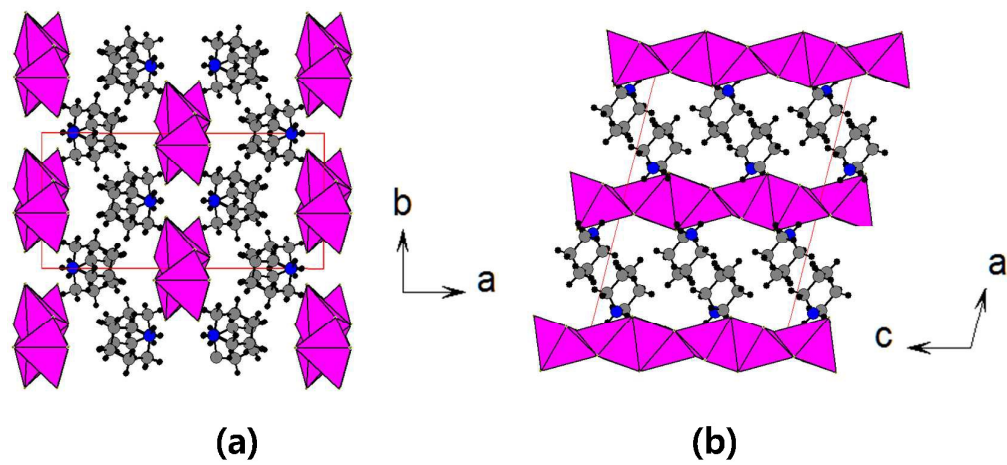
Figure 2.

Figure 3

Figure 4
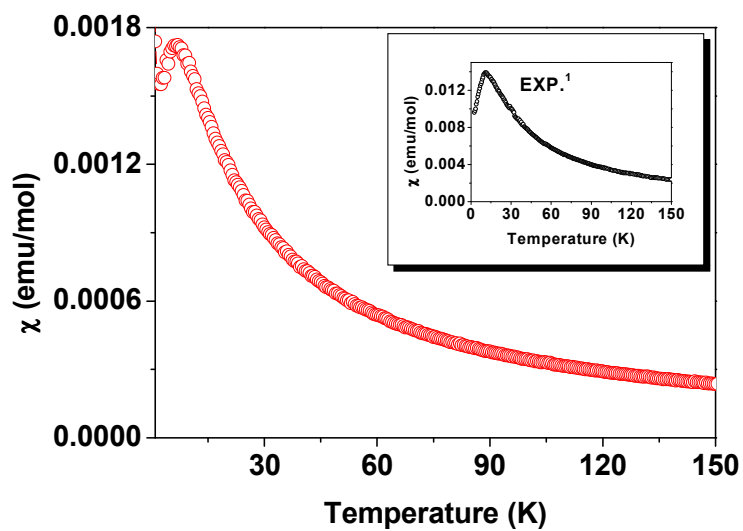
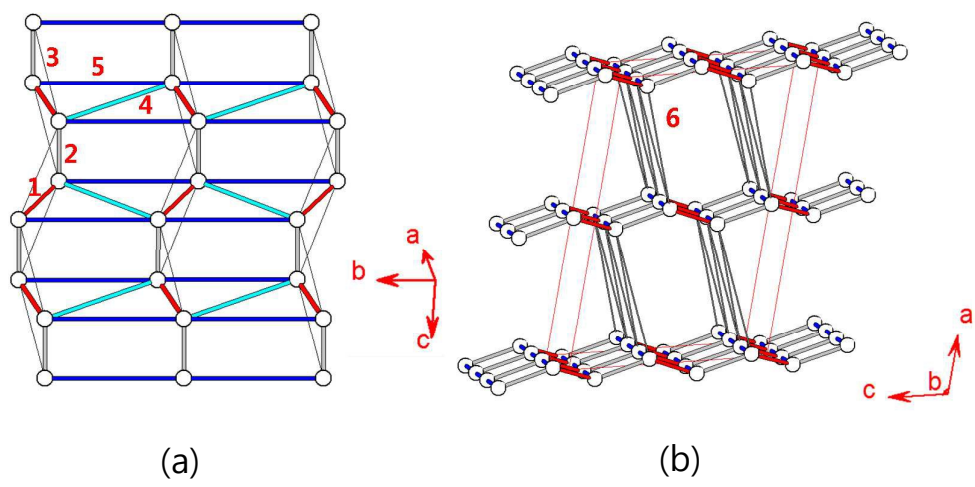(a)   (b)
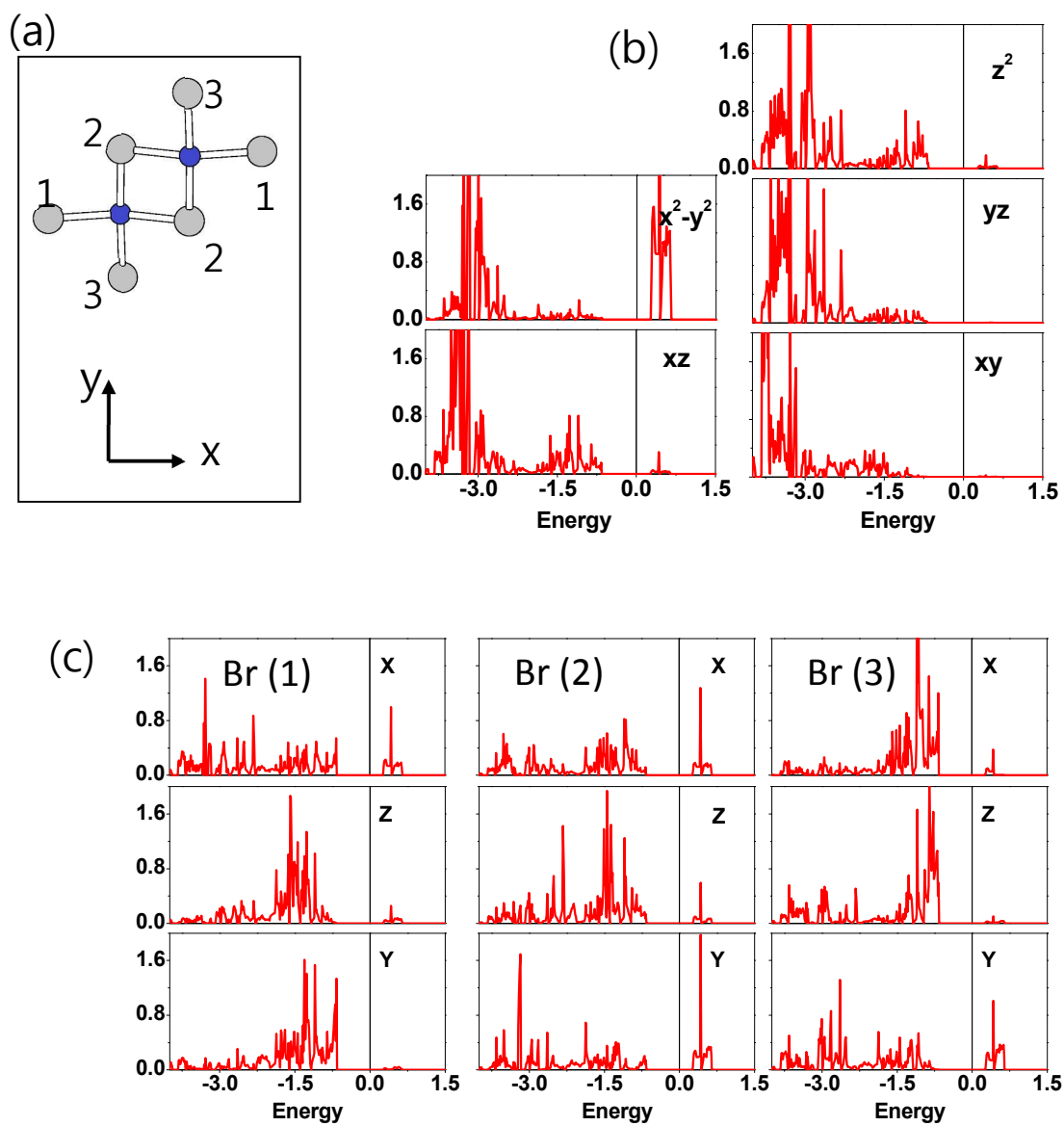
Figure 5.

(a)

(b)

(c)

Figure 6

Table of contents

The magnetic structure and magnetic anisotropy of $(C_5H_{12}N)CuBr_3$ were examined on the basis of density functional calculations. The uniform antiferromagnetic chain behavior observed for $(C_5H_{12}N)CuBr_3$ is not caused by the $CuBr_3$ chains, but by the interchain exchanges leading to two-leg spin ladders. The Cu^{2+} ions in $(C_5H_{12}N)CuBr_3$ have easy-axis anisotropy, and this arises largely from the spin-orbit coupling of the Br^- ligands.